Metallophysics and Advanced Technologies
Металофіз. новітні технол.
Metallofiz. Noveishie Tekhnol.
2022, vol. 44, No. 3, pp. 327–342
https://doi.org/10.15407/mfint.44.03.0327
Reprints available directly from the publisher

PACS numbers: 61.05.C-, 61.66.Dk, 66.48.Dc, 75.50.Vv, 75.60.Ej, 86.20.Ev

Comparative Study of Cubic NiC_x ($x \approx 0.33$) Formation Kinetics under Mechanical Alloying of Ni–CNT and Ni–Graphite Charge

O. Nakonechna, K. Ivanenko*, A. Kuryliuk, and N. Belyavina

Taras Shevchenko National University of Kyiv,
60 Volodymyrska Str.,
UA-01033 Kyiv, Ukraine
**Institute of Macromolecular Chemistry, N.A.S. of Ukraine,*
48 Kharkiv Highway,
UA-02160 Kyiv, Ukraine

Mechanical alloying of the elemental powder mixture of nickel–multiwalled carbon nanotubes (Ni–CNT) and nickel–spectroscopic grade graphite (Ni–SGG) is performed in a high energy planetary ball mill under the same technological modes. Nanocrystalline NiC_x carbide (x = 0.3–0.4) synthesized is examined by X-ray diffraction methods (phase and structural analysis, determination of the real structure parameters, *etc*.). The carbides synthesized are ferromagnets, the coercive force of which (H_c = 6–12 kA/m) depends on the amount of interstitial carbon atoms in octahedral voids of Ni crystal lattice. It is shown that an allotropic form of carbon (SGG or CNT) used at mechanical alloying effects the charge components interaction as well as the crystal structure and properties of final synthesis products.

Key words: mechanical alloying, crystal structure, X-ray diffraction, carbon nanotubes, coercive force.

Для дослідження впливу різної алотропної форми вуглецевої компоненти на кінетику формування фаз під час механічного легування проведено серію експериментів з розмелювання порошкових сумішей нікель–багатостінні вуглецеві нанотрубки (Ni–ВНТ) та нікель–спектрально чистий графіт (Ni–SGG) у високоенергетичному планетарному млині. Синтезований у результаті такої обробки нанокристалічний карбід NiC_x

Corresponding author: Olesya Ivanivna Nakonechna
E-mail: olesya.nakonechna@knu.ua; lesnak4@gmail.com

Citation: O. Nakonechna, K. Ivanenko, A. Kuryliuk, and N. Belyavina, Comparative Study of Cubic NiC_x ($x \approx 0.33$) Formation Kinetics under Mechanical Alloying of Ni–CNT and Ni–Graphite Charge, *Metallofiz. Noveishie Tekhnol.*, **44**, No. 3: 327–342 (2022).
DOI: 10.15407/mfint.44.03.0327

($x = 0{,}3–0{,}4$) досліджували методами рентґенівської дифракції (фазовий та структурний аналіз, визначення реальних параметрів структури тощо). Синтезовані карбіди виявилися феромагнетиками, коерцитивна сила яких ($H_c = 6–12$ кА/м) залежить від кількості міжвузлових атомів Карбону в октаедричних порах кристалічної ґратниці Ni. Показано, що алотропна форма Карбону (SGG або BHT), яку застосовують під час механічного леґування, впливає на взаємодію компонентів шихти, а також на кристалічну структуру та властивості кінцевих продуктів синтезу.

Ключові слова: механічне леґування, кристалічна структура, рентґенівська дифракція, вуглецева нанотрубка, коерцитивна сила.

(Received March 13, 2021; in final version, December 10, 2021)

1. INTRODUCTION

Magnetic nanoparticle (NP) based materials have broad application prospects in the fields of magnetism, biomedicine, energy and biosensor technology. Such NPs ability as penetration deep into tissue and cells of living body has increased their potential for molecular diagnostics (as magnetically active marker medication) and for the targeted drug delivery [1–3]. Ni NPs could have taken a special place among nanomaterials in medicine. However, research have shown that Ni NPs cause a variety of toxic effects on cells, animals and humans and have toxic effects of multiple systems such as respiratory, cardiovascular and reproductive systems. Ni NPs can lead to oxidative stress, apoptosis, DNA damage and inflammation, and induce the increase of intracellular reactive oxygen [4]. Over the last decades, great effort has done into using of magnetic NPs in biosensor technologies for applications in different fields such as disease diagnosis and detection of pollutants in water and food. As a result of such studies a nickel nanoparticles-loaded three-dimensional porous magnetic graphene-like nanocomposite (NiNPs/3D-PMG) is created [5]. Furthermore, a sensor on its base has been successfully utilized to detect glucose in human serum with satisfactory results [5]. Besides, Ni NPs sensor can find its applications as a potential electrode material for the qualitative and quantitative analysis of Penicillin G in liquid samples [6], while capsulated Ni–C microspheres showed a great capability to use as an adsorbent of organic pollutants in different samples [7]. Considering the application prospects of encapsulated Ni–C NPs, it would be beneficial to develop magnetic nanomaterial, in which carbon atoms are placed directly into the nickel crystal lattice, forming the nickel carbide.

It is known that mechanical alloying of powders in a high-energy planetary ball mill is an effective method to obtain nanoscaled carbides. Previously we have successfully applied this method to synthesize such carbides as TiC, ZrC, HfC, VC, NbC, TaC, Mo_2C, W_2C, WC,

Fe_3C and Co_3C using the multiwalled carbon nanotubes (CNT) as the carbon component of a charge [8, 9]. V. K. Portnoi *et al.* [10] have obtained hexagonal Ni_3C carbide by mechanical alloying of the Ni–graphite charge (3:1). However, we synthesized Ni_3C carbide with a defective cubic lattice of ZnS sphalerite type as a result of Ni–CNT charge (3:1) processing [11]. This discrepancy prompted us to study the kinetics of simultaneous mechanical alloying of Ni–CNT and Ni-graphite charges.

Here we present the results of structural research and magnetic characteristics of nanomaterials synthesized.

2. EXPERIMENTAL DETAILS

2.1. Materials

Elemental Ni powder (99.9% wt. purity, particle size <80 μm), spectroscopic grade graphite powder (spectral purity 99.99%, particle size is less than 50 μm) and multiwalled CNT are used to prepare four starting charges of Ni–CNT and Ni–SGG systems. Multiwalled carbon nanotubes used in this study are synthesized by the catalytic chemical vapor deposition method (CVD) at TM Spetzmash Ltd. (Kyiv, Ukraine). Charge content is listed in Table 1.

2.2. Mechanical Alloying

Charges are sieved into four steel vials (70 mm height, 50 mm diameter) for simultaneous cyclic mechanical alloying in a high energy planetary ball mill (15 min of milling and 30 min of cooling) in argon atmosphere. Hardened steel balls (11 units of 15 mm diameter) and a ball-to-powder weight ratio of 40:1 are used. The vial temperature is held at below 375 K during the experiments by air cooling. The rotation speed is equal to 1480 rpm.

TABLE 1. Charge content for mechanical alloying.

Charge	at.%			% wt.		
	Ni	CNT	Graphite	Ni	CNT	Graphite
1	75	25	–	93.62	6.38	–
2	60	40	–	88.00	22.0	–
3	75	–	25	93.62	–	6.38
4	60	–	40	88.00	–	22.0

2.3. Characterization

Phase transformations of Ni–CNT and Ni–SGG charges at mechanical alloying have been studied by X-ray diffraction (XRD) methods on the test samples selected after every 30–60 min of milling. XRD data is collected with DRON-3M and Shimadzu XRD-6000 automatic diffractometers (CuK_α radiation) in a discrete mode. To implement the possibility of express research of test samples immediately after their selection from the reaction zone of a mill, the acquisition parameters of diffraction data are optimized to ensure the correctness of results obtained at sufficiently short exposure time: observation range $2\theta = (20–100)^\circ$, step scan of 0.05° and counting time per step at 3 s. The original software package, including full complex of standard Rietveld procedures, has been used for analysis and interpretation of the X-ray diffraction patterns obtained, namely, determination of peak positions and integral intensities of the Bragg reflections by means of full profile analysis; carrying out qualitative and quantitative phase analysis using PDF data for phase identification and the least square method for lattice parameters refinement; testing of the structure models and refining crystal structure parameters (including coordinates of atoms, atomic position filling, texture, *etc*.); calculation of the parameters of the real structure of the individual phases (coherent block sizes and microdeformation values) [12]. Parameters of crystal structure are refined for each phase presented in the selected test samples. The criteria for structural calculations correctness are the values of R_B and R_W reliability factors, not exceeding 0.015 in this study, as well as graphical form of the difference curve, illustrating the coincidence of the experimental diffraction pattern with the diffraction pattern reproduced on the basis of structural calculations performed. Deformation of the crystal lattice is calculated by the approximation method using as a reference a sample of compacted nickel metal (E = 202 GPa, $\nu = 0.28$). Residual stresses are calculated by the shifting of the diffraction reflections (predominantly, (022)), which substantially shifted from their positions calculated for the specific test sample.

Morphology of the final mechanically alloyed samples is studied by the scanning electron microscopy technique (SEM, JEOL JAMP-9500F, Japan). JEOL JAMP-9500F is a field emission auger microprobe operated at 10 kV, which offers the flexibility of optional analysis functions such as energy-dispersive X-ray spectroscopy (EDS).

Vibration magnetometer (the vibration frequency of 70 Hz) is used to examine the magnetic properties of test samples. Measurements are provided in a constant magnetic field of up to 200 kA/m. The experimental error is less than 5%.

The Vickers microhardness tests are performed with PMT-3 apparatus at room temperature. All samples are preliminary polished by

diamond paste. The load of 150 g is applied to the sample for 15 s. Number of indentations per one sample is 50.

3. RESULTS AND DISCUSSION

3.1. Kinetics of Mechanical Alloying of Ni–CNT and Ni–SGG Charges

X-ray phase analysis indicates two phases coexist in a charge after 60 min of mechanical alloying of all samples, namely, initial nickel phase with lattice parameter a = 0.3522(3) nm and additional isostructural cubic phase (probably NiC_x) with higher lattice parameter (Fig. 1, *a*). This additional phase becomes the only constituent of the test samples (Fig. 1, *b*) with further processing (120 min and longer). Besides, its lattice parameter gradually increases with processing time, which can undoubtedly indicate the invasion of carbon atoms in the crystal structure of nickel (Fig. 2).

Study of the elemental composition of 800 min milled products by EDS method has revealed that the iron content (the main component of debris at milling) does not exceed 1–2% wt. Therefore, it doesn't make any contribution in the lattice parameter value of material synthesized (Fig. 2, *a*).

In order to determine the amount of carbon atoms embedded in the NiC_x phase, we considered several variants of their localization in the crystal lattice of nickel. First of all, the possibility of placing carbon atoms in the octahedral and/or tetrahedral voids of the f.c.c. nickel lattice is estimated to build a test model. As a result of structural cal-

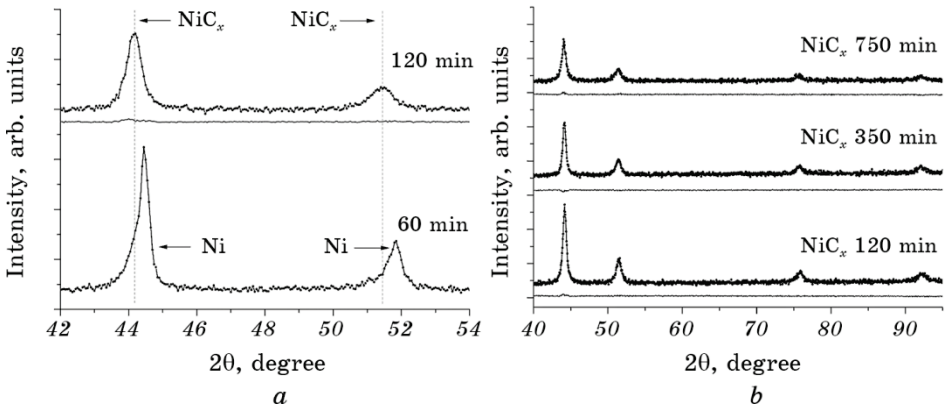

Fig. 1. Fragments of diffraction patterns (*a*) and difference curve illustrating the coincidence of experimental diffraction pattern with that reproduced on the basis of structural calculations performed (*b*) of the test samples selected after certain time of Ni–CNT (3:2) charge milling.

culations, it is shown that the carbon atoms are statistically located in the centres of tetrahedral voids of the nickel lattice at the initial stage of mechanical alloying of both Ni–CNT and Ni–SGG charges. Previously we showed similar arrangement of the carbon atoms in milled Ni–CNT (3:1) charge [11], which is typical to a placement of the sulfur atoms in ZnS sfalerite-type structure. *i.e.*, at the beginning of mechanical alloying (up to 350 min of milling) the crystal structure of the NiC_x phase is characterized by following arrangement of atoms: F-43m space group, 4Ni atoms in 4(a) 0 0 0 and qC atoms in 4(c) 1/4 1/4 1/4, where q is the calculated value of the position filling parameter. An amount of interstitial carbon atoms in nickel crystal lattice has calculated using q value obtained for each test sample (Fig. 2). The correctness of the structural calculations performed is evidenced by the difference curves (Fig. 1) as well as the reliability factor (Table 2). It should also be noted that such arrangement of carbon atoms is inherent to crystal structures of all NiC_x phases formed up to 300 min of processing (Fig. 2). For all NiC_x phases synthesized the limit value of the carbon atoms placed just in the centres of tetrahedral voids is about 20 at.%, which corresponds to one carbon atom per defective lattice of the ZnS sphalerite type (Fig. 2, a).

Figure 2 also shows typical knees at 350 min for all samples studied regardless of what type of carbon component is used in the charge (CNT or SGG). Moreover, all four test samples selected after 350 min of milling are characterized by similar lattice parameters $a \approx 0.355$ nm and carbon content of 23 at.% C ($x \approx 0.3$) (Table 2). Crystal data of the NiC_x phases in these samples, intended for further studies of their magnetic properties, are listed in Table 3.

Lattice parameters of 350 min milled NiC_x phases formed in samples with (3:2) charge ratio continue to increase significantly, while those

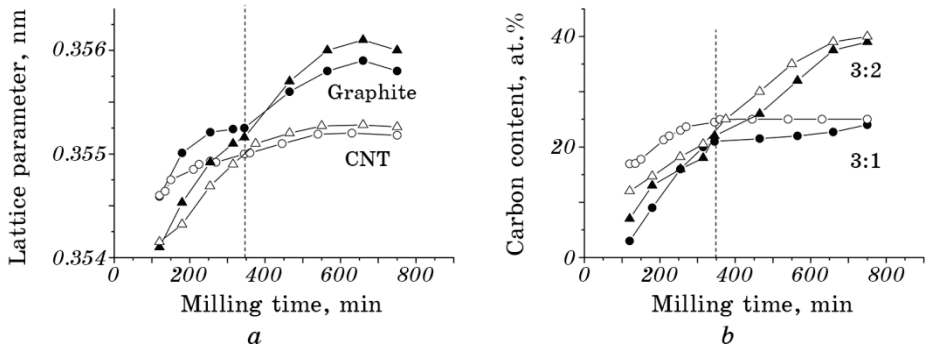

Fig. 2. Dependences of the carbon content and lattice parameters of NiC_x phase formed on the milling time. White symbols correspond to Ni–CNT charge, black symbols—to Ni–SGG charge; circles indicate (3:1) charge content, triangles—(3:2) content.

TABLE 2. Crystal structure data and real structure parameters for NiC_x carbide obtained after 350 min of milling.

Initial charge	Lattice parameter a, nm	Total amount of carbon C, at.%	Amount of carbon in voids, %*		Block size D, nm	Microdeformation of lattice $\Delta d/d$, %	Residual stresses L, GPa
			Tetra	Octa			
Ni powder	0.3521(1)	–	–	–	24	0.18	0.005
			(3:1) charge				
Ni–SGG	0.3552(1)	21(2)	97	3	11	0.26	0.182
Ni–CNT	0.3548(1)	23(2)	98	2	11	0.24	0.632
			(3:2) charge				
Ni–SGG	0.3552(1)	22(2)	90	10	10	0.45	0.006
Ni–CNT	0.3548(1)	25(2)	92	8	12	0.39	0.517

* The fraction of carbon atoms in tetra- and octahedral voids is calculated using an alternative model.

values in the samples with (3:1) ratio are rapidly saturated.

TABLE 3. Crystal data for NiC_x carbides formed in 350 min milled Ni–CNT and Ni–SGG charges (Space group F-43m (No. 216)).

Atom	Site	X	Y	Z	Site occupation	
					NiC_x phase (Ni–SGG (3:1) charge)	NiC_x phase (Ni–SGG (3:2) charge)
Ni	4a	0	0	0	1.00(1)	1.00(1)
C(1)	4c	0.25	0.25	0.25	0.256(3) (tetra void)	0.254(4) (tetra void)
C(2)	4b	0.5	0.5	0.5	0.008(3) (octa void)	0.028(4) (octa void)
Lattice parameter a, nm					0.3552(1)	0.3552(1)
Total isotropic B factor, nm^2					$2.15(2)\cdot10^{-2}$	$1.25(2)\cdot10^{-2}$
Calculated content, at.%					79(2) Ni + 21(2) C	78(2) Ni + 22(2) C
Reliability factor R_B					0.009	0.008
Atom	Site	X	Y	Z	Site occupation	
					NiC_x phase (Ni–CNT (3:1) charge)	NiC_x phase (Ni–CNT (3:2) charge)
Ni	4a	0	0	0	1.00(1)	1.00(1)
C(1)	4c	0.25	0.25	0.25	0.296(3) (tetra void)	0.307(4) (tetra void)
C(2)	4b	0.5	0.5	0.5	0.006(3) (octa void)	0.027(4) (octa void
Lattice parameter a, nm					0.3548(1)	0.3548(1)
Total isotropic B factor, nm^2					$1.68(3)\cdot10^{-2}$	$3.09(9)\cdot10^{-2}$
Calculated content, at.%					77(2) Ni + 23(2) C	75(2) Ni + 25(2) C
Reliability factor R_B					0.008	0.004

Structural calculations show that the trial models (with cubic or rhombohedral symmetry), in which the carbon atoms are displaced from the centre of tetrahedral voids (coordinates are equivalent to 1/4 1/4 1/4) to the centre of f.c.c. lattice (1/2 1/2 1/2) demonstrate the best agreement between experimental and calculated diffraction reflections intensities for these phases (reliability factor is less than 0.01). Here we consider a cubic model built in the same space group F-43m: 4Ni atoms in 4(a) 0 0 0 and qC atoms in 16(e) x x x, where the coordinate parameter x ($\approx$1/3) and q values are calculated for each 350 min milled NiC_x phase (Fig. 2). It is seen that the contents of NiC_x phases synthesized at mechanical alloying of four charges generally correspond to the compositions of source mixtures. Although the lattice parameters of NiC_x phases obtained from Ni–SGG charges are slightly higher than those obtained from Ni–CNT ones (Fig. 2). The pattern of atoms arrangement in NiC_x phases formed after 350 min of milling is presented at Fig. 3, *b*. One can see that the carbon atoms statistically occupy the vertices of tetrahedrons, which centres are the centres of tetrahedral voids.

An alternative to two models described above may be their common model build within the space group F-43m, in which carbon atoms are statistically placed at the centres of both tetrahedral and octahedral voids, namely, 4Ni atoms in 4(a) 0 0 0, qC atoms in 4(c) 1/4 1/4 1/4 and q'C atoms in 4(b) 1/2 1/2 1/2, where q and q' are the fillings of corresponding 4(c) and 4(b) positions by carbon atoms. It should be noted that q' is equal to 0 for NiC_x phase formed at the beginning of mechanical alloying. In general, the agreement between experimental and calculated intensity of reflections is better for the model presented in Fig. 3, *b* than for this alternative model.

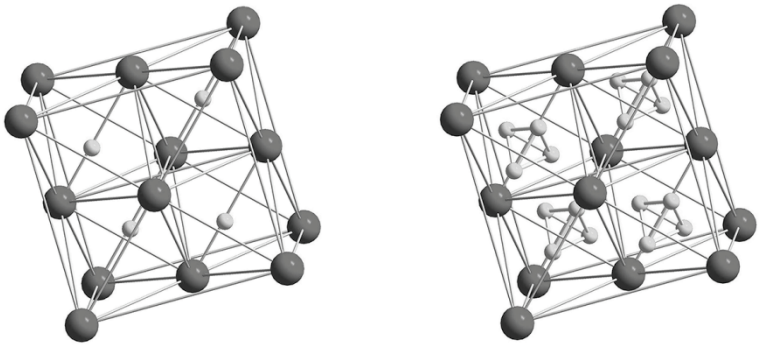

Fig. 3. Arrangement of atoms in mechanically alloyed NiC_x carbides: NiC_x phase containing up to 20 at.% C (*a*); NiC_x phase containing more than 20 at.% C (*b*). Nickel atoms are marked as big grey circles and carbon atoms are marked as small light grey circles.

Parameters of real structure (coherent scattering block size D, microdeformation of crystal lattice $\varepsilon = \Delta d/d$) and the residual stresses value $L = E/\nu((d - d_0)/d_0)$ are calculated for each NiC_x phases obtained taking into account that all reflections at the diffraction patterns are significantly broadened and some of them (mostly (022) reflection) are also significantly shifted. In order to estimate available shift of the position, this reflection is excluded from the refinement of lattice parameter a by the least square method. Subsequently, the value of d_0 is calculated using the lattice parameter for the reflection (022), and the value of this reflection is taken experimentally as the value of d. The fact that (022) reflection turned out to be the most sensitive to deformation is, in our opinion, natural because the carbon atom is located in this plane in the centres of tetrahedral voids when embedded in Ni crystal lattice according to structural studies.

As a result of the calculations performed, it is shown that D value for NiC_x phases is practically independent on the milling time and charge content and is equal to 8–12 nm for all synthesis products. However, ε and L values for these phases are changed (Fig. 4).

Thus, the study provided has shown that 350 min milled test samples are characterized by close values of the lattice parameters of NiC_x phase formed and close amount of carbon atoms solved (Fig. 2). Moreover, the carbon atoms in these carbides are localized mainly in the centres of the tetrahedral voids (Fig. 3, *a*). SEM analysis of the test samples selected after 350 min of milling demonstrates a similarity in their morphology. Namely, all powders studied consist of individual small particles and agglomerates of such particles (Fig. 5). EDS analysis confirms XRD data on the amount of carbon atoms solved in nickel lattice (about 23 at.%), which is close to the composition of the Ni_3C carbide.

Thus, taking into account the similarity of crystallographic charac-

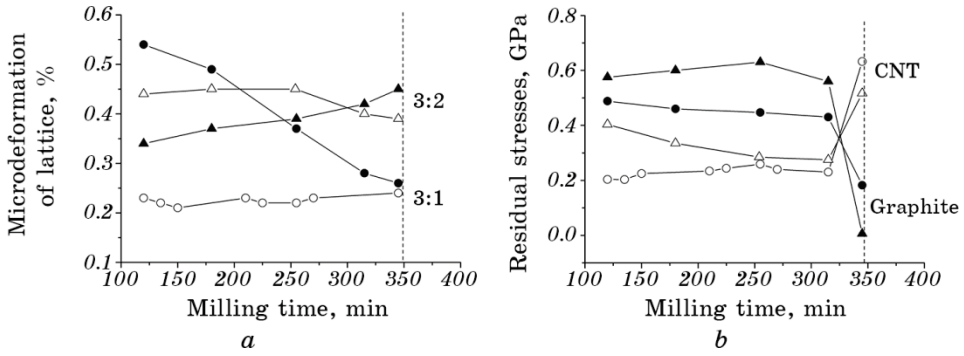

Fig. 4. Microdeformation and residual stresses of the crystal lattice for NiC_x phases in dependence on milling time. Symbols correspond to Fig. 2.

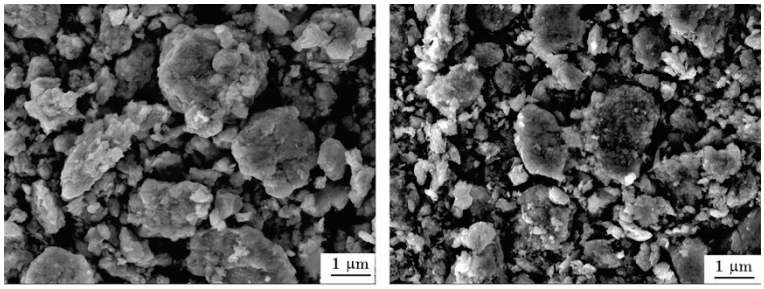

a *b*

Fig. 5. SEM images of the 350 min milled samples: Ni–CNT charge (3:1) (*a*); Ni–SGG charge (3:1) (*b*). ×10000.

teristics and compositions of NiC_x phases synthesized (Table 2, 3), the magnetic properties are studied for the test samples selected just after 350 min of processing in a ball mill.

3.2. Magnetic Characteristics of 350 min Milled NiC_x Phases Formed in Ni–CNT and Ni–SGG Charges

Test samples selected after 350 min of mechanical alloying of charges are examined using a vibration magnetometer. All the materials studied are ferromagnets, the hysteresis loops of which are shown in Fig. 6, magnetic parameters calculated from these loops are listed in Table 4.

As it can be seen from Figure 6, the charge content used affects not only the shape of the hysteresis loops, but also the magnetic characteristics of the NiC_x carbide with $x \approx 0.33$ (21–25 at.% C) existing in each of four test samples. Thus, the coercive force H_c of cubic $NiC_{0.33}$ carbide (close to stoichiometric Ni_3C composition) varies within 4–12 kA/m with residual magnetization M_R (7–9 $A \cdot m^3/kg$) and almost constant value of saturation field H_S (76.5 kA/m) (Table 4).

Analyzing the characteristics obtained, we can conclude that $NiC_{0.33}$ carbide synthesized keeps the ferromagnetic features of nanocrystalline nickel powder (Table 4), and H_c value is close to that predicted by L. Yue *et al.* [13] for disordered Ni_3C carbide. It should be noted that nanocrystalline nickel powder is obtained by milling initial Ni powder in a high-energy planetary ball mill under the same conditions as Ni–CNT and Ni–SGG charges.

It is known that the coercive force depends strongly on the grain size of the material [14]. Wherein, since grain boundaries act as impediments to domain wall motion, coercive force increases with decreasing grain size. Taking into account that the effective width of the domain wall for nanocrystalline nickel is about 40 nm [14] while the crystallite size of powders synthesized in this work are much smaller (10–12 nm,

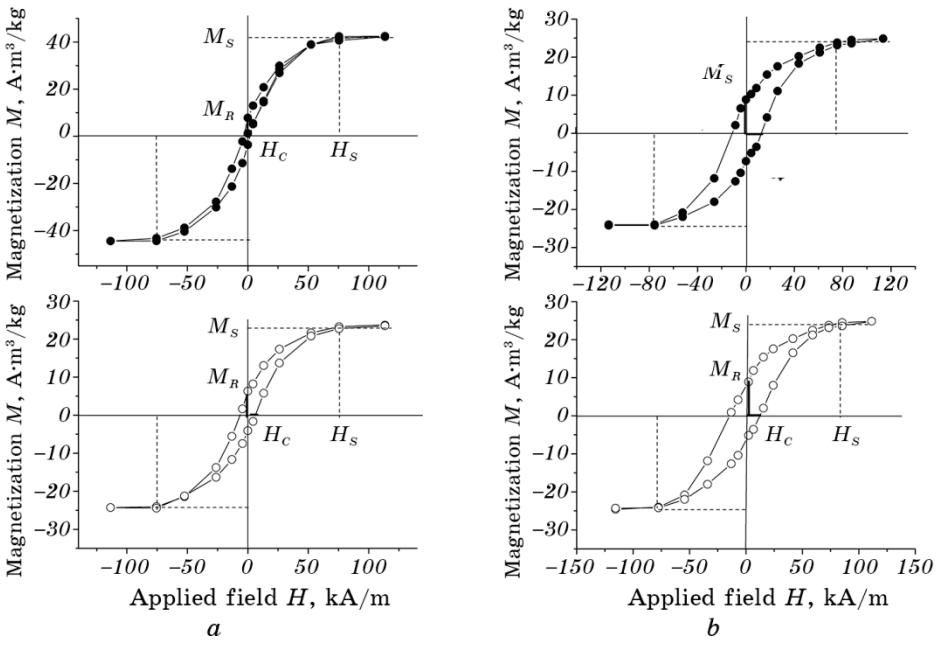

Fig. 6. Hysteresis loops of the 350 min milled test samples: Ni–SGG charge (black circles) and Ni–CNT charge (white circles), charge composition (3:1) (*a*) and (3:2) (*b*).

Table 2), we assume that other factors affect H_c value of $NiC_{0.33}$ carbide synthesized.

Analysis of the crystal and real structure parameters of $NiC_{0.33}$ car-

TABLE 4. Magnetic characteristics of NiC_x carbide obtained after 350 min of mechanical alloying.

Initial charge	Coercive force H_c, kA/m	Residual magnetization M_R, A·m³/kg	Saturation magnetization M_S, A·m³/kg	Saturation field H_S, kA/m
Ni_3C disordered [13]	5.7	–	–	–
Ni–nanopowder [14]	1.2	–	–	–
Ni–nanocrystalline	2.2	3.0	40.6	76.5
(3:1) charge composition				
Ni–SGG	3.8	7.8	41.9	76.3
Ni–CNT	5.7	6.6	23.1	76.9
(3:2) charge composition				
Ni–SGG	12.1	8.6	24.1	76.5
Ni–CNT	11.7	8.5	22.4	76.9

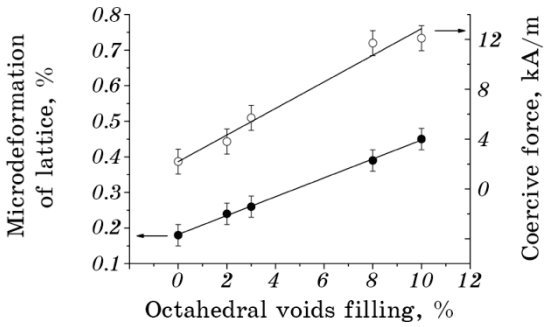

Fig. 7. Microdeformation of the crystal lattice and coercive force of the cubic $NiC_{0.33}$ carbide in dependence on filling of octahedral voids of Ni crystal lattice.

bide synthesized and its magnetic characteristics (Tables 2, 3) allows us to conclude that increase in the amount of carbon atoms embedded in octahedral voids of nickel structure causes an increase in the microdeformation degree of carbide lattice, which, in turn, contributes to an increase in H_c value (Fig. 7). It should be noted that the amount of carbon atoms located in the octahedral voids of the cubic $NiC_{0.33}$ structure is calculated using the alternative model described above (Table 2).

In general, the values of coercive force and the shape of hysteresis loop (Fig. 6, Table 2) certify that nanocrystalline $NiC_{0.33}$ (cubic Ni_3C carbide) synthesized here belongs to semi-hard magnetic materials ($H_c > 4$ kA/m).

4. DISCUSSION

Comprehensive study of Ni–SGG and Ni–CNT powders mechanically alloyed in a high-energy planetary ball mill at identical technological conditions has revealed both similarities and differences in the formation of NiC_x carbide with ZnS sphalerite defective structure.

It is known that both CNT and SGG source powders are gradually amorphized (up to 60 min of milling) at the initial stage of the mechanical alloying [15, 16]. Active interaction of carbon and nickel powder begins after amorphization process is completed. Therefore, the initial nickel powder is the main counterpart for all samples processed up to 100 min (with some amount of graphite in the Ni–SGG charge).

An increase of the Ni lattice parameters is observed in test samples milled for 100 min or longer (Fig. 2). It is noteworthy that at the initial stage of processing the lattice parameter of NiC_x phase synthesized from Ni–SGG charge is slightly higher than that synthesized from Ni–CNT charge, although the content of carbon embedded in NiC_x is lower in the case of Ni–SGG charge (Fig. 2). Similarity in a values and compositions is observed only for the NiC_x formed in 350 min milled test

samples. Saturation process of the NiC_x crystal lattice with carbon atoms continues with further milling for charge (3:2), in contrast to charge (3:1).

Considering our previous TEM studies of the Fe_3C carbide formation at mechanical alloying of Fe–CNT charge [8], one can assume that similar processes are realized at the formation of NiC_x carbide. Amorphized carbon powder wraps nickel particles and penetrates into them along grain boundaries and dislocations. This process dominates when the charge is mechanically alloyed for up to 100 min. Further processing leads to a gradual nucleation of NiC_x carbide phase, formation of which begins on the surface of nickel particles. Moreover, a shell formed on such nickel particles leads to appearance of surface tension (residual stresses, Fig. 4). Upon reaching a certain thickness, this shell, formed by the products of the synthesis of the NiC_x phase exfoliates, which is clearly illustrated by Fig. 4, where the obtained values of residual stresses are minimal at 315–350 min of processing, ie, upon completion of the formation of defective ZnS sphalerite structure.

N. Kundan *et al.* [17] have described similar process of carbon atoms solution in nickel crystal lattice at mechanical alloying of the Ni–graphite charge. Unfortunately, authors of Ref. [17] have not defined the exact location of carbon atoms in nickel lattice, taking as a basis the common idea of its localization in octahedral voids by analogy with the NaCl-type structure. However, our previous studies on mechanical alloying of Ni–CNT charge [9] have shown that such localization of carbon atoms is characteristic of a nickel-based solid solution with low CNT content (up to 5 at.%).

Structural calculations performed here have revealed that the NiC_x phase with a defective ZnS sphalerite structure is formed at the first stage of mechanical alloying of both Ni–SGG and Ni–CNT charges. Presumably, this phase appears to be an individual compound (as evidenced by the two-phased nature of some test samples selected at up to 100 min of processing). Moreover, the existence region of this phase can extend beyond 40 at.% of carbon, which is shown by N. Kundan *et al.* [17].

Considering the fact that the crystal lattice of nickel is faster saturated with carbon atoms and the lattice period of NiC_x formed is lower in a case of Ni–CNT charge milling one can conclude that both the effective radius of amorphized CNTs and their diffusion rate are somewhat higher than those for amorphized graphite. Moreover, the formation of NiC_x from the Ni–CNT charge proceeds more smoothly as evidenced by independence of the carbide real structure parameters on the milling time. No knees on $a(t)$ dependence (Fig. 2, *a*) and on the dependence of lattice parameter on the carbon content embedded into the nickel crystal lattice (Fig. 8) supplementary imply smooth behaviour of NiC_x formation from Ni–CNT charge. Concurrently, well-defined

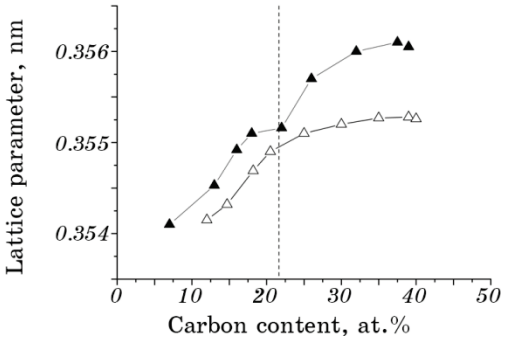

Fig. 8. Dependence of the lattice parameters of NiC_x formed in the charges of (3:2) content. Ni–SGG (black triangles) and the Ni–CNT charge (white triangles).

knees are visible on the same dependences for Ni–SGG charge in the vicinity of 20–22 at.% C. In our opinion these features are caused by a change of the carbide crystal structure. A similar dependence of the lattice parameters of the synthesized phase is observed by N. Kundan *et al.* [17].

It should be necessary to note that indeed mechanical alloying results in a (Ni, C) solid solution formation with octahedral occupation of carbon atoms at a low carbon content (up to 5 at.% C) [9]. However, considering the calculation of electronic structure parameters the preferred arrangement of carbon atoms in the tetrahedral voids is shown for the cubic NiC_x phase, which contains more than one carbon atom per unit cell [18]. This factor can support conclusion that the NiC_x phase studied is individual carbide and not a solid solution based on a nickel lattice. Although to absolutely confirm the conclusion on the existence of an individual NiC_x carbide, an additional experimental study of mechanical alloying of Ni–C charge containing up to 25 at.% carbon is needed.

In order to study the mechanical properties of NiC_x carbide the 350 min milled Ni–CNT charge (3:1) is sintered by high pressure–high temperature (HP–HT) technique. The toroid type high pressure apparatus is used to create the pressure of 8 GPa and temperature of 1200°C and 1500°C (the test sample powder wrapped into the graphite foil is treated in a high pressure cell during 40 s).

It appeared to be that NiC_x phase with a defective structure of ZnS-sphalerite with a = 0.3543–0.3548 nm is the only constituent of bulk samples. The fraction x of carbon atoms in the compacted HP–HT samples varies from 0.33 to 0.44, which may be caused by the addition of extra carbon atoms from the graphite shell used in HP–HT reaction.

Average value of the Vickers microhardness for sintered NiC_x samples (6.9–7.2 GPa) is significantly higher compared to microhardness of bulk metallic Ni (0.638 GPa).

5. CONCLUSION

A comprehensive study of mechanically alloyed under the same technological modes Ni–CNT and Ni–SGG charges has revealed the following:
1. A nanocrystalline cubic carbide NiC_x ($x = 0.3–0.7$) is synthesized for the first time at mechanical alloying of both Ni–CNT and Ni–SGG charges. According to XRD data the crystal structure of this NiC_x phase belongs to ZnS sphalerite type with partial filling of its tetrahedral voids by carbon atoms.
2. Kinetics of the NiC_x carbide formation is studied by XRD methods. First of all, the features of Ni lattice parameter caused by the increase of the carbon atoms embedded have revealed and the changes of microdeformation as well as residual stresses of NiC_x crystal lattice have analyzed.
3. It is shown that NiC_x carbides synthesized after 350 min of milling both Ni–SGG and Ni–CNT charges exhibit similar crystal structure and composition. The materials obtained are ferromagnets, the coercive force of which depends on the amount of the carbon atoms additionally embedded in the octahedral voids of the nickel crystal lattice.
4. It is shown that crystal structure of final synthesis product as well as interaction between the initial charge components are affected by allotropic form of carbon (graphite or carbon nanotubes) used.

ACKNOWLEDGEMENT

The work is financially supported by the State budget of Ukraine *via* Ministry of Education and Science of Ukraine (grant No. 0119U100184).

REFERENCES

1. D. Lisjak and A. Mertelj, *Prog. Mater. Sci.*, **95**: 286 (2018).
2. R. Saini, S. Saini, and S. Sharma, *J. Cutaneous Aesthetic Surgery*, **3**, Iss. 1: 32 (2010).
3. Y. Li and H. Zhang, *J. Biomedical Nanotechnology*, **15**, No. 1: 1 (2019).
4. Y. Wu and L. Kong, *Environ. Geochem. Health*, **42**, No. 7: 2277 (2020).
5. F. Wang, Y. Feng, S. He, L. Wang, M. Guo, Y. Cao, Y. Wang, and Y. Yu, *Microchemical J.*, **155**:104748 (2020).
6. S. Salihu, N. Yusof, F. Mohammad, J. Abdullah, and H. A. Al-Lohedan, *Journal of Nanomaterials*, 2019, Article ID 1784154 (2019).
7. L. Hao, X. Meng, C. Wang, Q. Wu, and Z. Wang, *J. Chromatography A*, **1605**: 460364 (2019).
8. O. Boshko, O. Nakonechna, N. Belyavina, M. Dashevskyi, and S. Revo, *Adv. Powder Technol.*, **28**, No. 3: 964 (2017).
9. O. I. Nakonechna, M. M. Dashevskyi, O. I. Boshko, V. V. Zavodyanny, and N. N. Belyavina, *Prog. Phys. Metals*, **20**, No. 1: 5 (2019).

10. V. K. Portnoi, A. V. Leonov, S. N. Mudretsova, and S. A. Fedotov, *The Physics of Metals and Metallography*, **109**, No. 2: 153 (2010).
11. O. I. Nakonechna, N. N. Belyavina, M. M. Dashevskyi, A. M. Kuryliuk, and V. A. Makara, *Dopovidi Natsionalnoy Akademii Nauk Ukrainy*, No. 4: 50 (2019) (in Ukrainian).
12. M. Dashevskyi, O. Boshko, O. Nakonechna, and N. Belyavina, *Metallofiz. Noveishie Tekhnol.*, **39**, No. 4: 541 (2017).
13. L. Yue, R. Sabiryanov, E. M. Kirkpatrick, and D. L. Leslie-Pelecky, *Phys. Rev. B*, **62**, No. 13: 8969 (2000).
14. J. F. Loffler and W. Wagner, *Phys. Rev. B*, **57**, No. 5: 2915 (1998).
15. Y. B. Li, B. Q. Wei, J. Liang, Q. Yu, and D. H. Wu, *Carbon*, **37**: 493 (1999).
16. R. M. Nikonova, N. S. Larionova, V. I. Ladyanov, V. V. Aksenova, A. D. Rud, and I. M. Kirian, *J. Alloys Compd.*, **682**: 61 (2016).
17. N. Kundan, P. Biswajit, A. K. Keshri, and P. R. Soni, *Int. J. Minerals, Metall. Mater.*, **26**, No. 8: 1031 (2019).
18. O. I. Nakonechna, K. O. Ivanenko, A. M. Kuryliuk, and N. N. Belyavina, *Phys. Chem. Solid State*, **22**, No. 1: 59 (2021).